



Exceptional adsorption properties of amino-carboxylic acid chelating fibers for calcium, magnesium, and strontium ions

Da-Xin Liu^a, Gang Xu^{a,c}, Zhao-Wen Chen^b, Li Wang^b, Ming-Hong Wu^{a,*}

^aSchool of Environmental and Chemical Engineering, Shanghai University, Shanghai 200444, P.R. China, emails: mhwu@shu.edu.cn (M.-H. Wu), 1967145467@qq.com (D.-X. Liu), xugang@shu.edu.cn (G. Xu)

^bPurification Equipment Research Institute of CSIC, Zhanlan Road 1, Handan 056027, P.R. China, emails: 18634101913@163.com (Z.-W. Chen), wangli2607@163.com (M.-H. Wu)

^cKey Laboratory of Organic Compound Pollution Control Engineering, Ministry of Education, Shanghai 200444, P.R. China

Received 19 April 2023; Accepted 30 August 2023

ABSTRACT

In the chlor-alkali industry, the thorough purification of calcium (Ca^{2+}), magnesium (Mg^{2+}), and strontium ions (Sr^{2+}) presents a considerable challenge. In this context, we developed novel amino carboxylic acid fibers in this study by using laboratory-synthesized polyacrylonitrile–polyethyleneimine amino fibers as the matrix. The amino carboxylation process was achieved by introducing chloroacetic acid under mild alkaline and heating conditions, resulting in the desired amino carboxylic acid fibers (PAN-C-Na). Adsorption experiments demonstrated that the PAN-C-Na fibers reached adsorption equilibrium within 30 s. Additionally, they effectively adsorbed Ca^{2+} and Mg^{2+} ions at ultralow concentrations (<0.02 mg/L), exhibiting outstanding adsorption capacities of 0.40 and 0.36 mmol/g, respectively, and exceeding 50% of their saturation adsorption capacities. Moreover, compared to amino-phosphonic acid fibers, which are another type of calcium–magnesium adsorptive fibers, the PAN-C-Na fibers exhibited twice the selectivity for Sr^{2+} adsorption and proved effective in eliminating residual Sr^{2+} in brine. These findings highlight the potential of PAN-C-Na fibers as a promising material for the thorough purification of Ca^{2+} , Mg^{2+} , and Sr^{2+} ions in the chlor-alkali industry.

Keywords: Amino carboxylic acid fibers; Chelation; Calcium; Magnesium; Strontium; Rapid adsorption

1. Introduction

To address the urgent issue of global climate change, China, a leading carbon emitter, has introduced its “dual carbon” strategy to peak CO_2 emissions by 2030 and attain carbon neutrality by 2060. To meet these ambitious goals, optimizing and modernizing energy-intensive industries is essential to enhance energy efficiency and reduce carbon emissions. Among these industries, caustic soda production has undergone substantial upgrades and transformations, resulting in reduced energy consumption and emissions. China has now fully transitioned its caustic soda production to ion-membrane technology, but this shift has resulted in stricter quality

requirements for saltwater purification. Ensuring high-quality saltwater is critical as low-quality saltwater can shorten the lifespan of ion membranes. Moreover, if contaminants such as Ca^{2+} , Mg^{2+} , and Sr^{2+} are not efficiently removed during the saltwater purification process, they can cause severe damage to the ion-membrane caustic soda electrolysis equipment [1–3]. Additionally, maintaining the appropriate concentration of Ca^{2+} and Mg^{2+} is vital for achieving a high current efficiency at elevated current densities. Prolonged exposure to saltwater with high impurity levels can lead to increased membrane resistance, elevated cell voltage, reduced current efficiency, and enhanced energy consumption. Consequently, reducing the concentration of Ca^{2+} and Mg^{2+}

* Corresponding author.

in purified saltwater has become an urgent matter requiring immediate attention.

Numerous techniques, including the use of ion exchange resins [4–14], reverse osmosis [15–19], electrodialysis [20–24], lime softening [25,26], nanofiltration [27–31], chelating resins [32], membrane separation technology [33–36], and distillation [37–39], have been developed for the removal of Ca^{2+} and Mg^{2+} from water. Each of these approaches operates uniquely and possesses its own set of advantages and limitations. In the brine secondary refining process used in the chlor-alkali industry, chelating resins are commonly employed to remove Ca^{2+} and Mg^{2+} ions with concentrations of 1 ppm or less from large volumes of water. The primary chelating groups used in these resins are amino carboxylic acids and aminophosphonic acids.

Existing research and improvements, such as those involving Lewatit ion-exchange resins from Lanxess, have focused on increasing the specific surface area or altering the bead diameter of existing resins [40]. However, the effectiveness of these enhancements is limited. Consequently, we propose the use of chelating fibers instead of resins. Chelating fibers represent the next generation of materials after resins and are particularly well-suited for the effective treatment of low-concentration ions. Compared to resin matrices, fibers have smaller diameters, which facilitate faster membrane and intraparticle diffusion. These fibers can be prepared by modifying matrix fibers using spinning technology, allowing for adjustments in fiber structure and morphology by controlling parameters such as spinning temperature and stretching rate, which in turn affect their surface properties. In contrast to resins, wherein functional groups are evenly distributed, chelating fibers have more concentrated functional groups on their surface, granting them rapid adsorption capabilities. In cases requiring trace-ion removal, kinetic performance takes precedence over reaction equilibrium constants, as processing time is typically prioritized. Therefore, reaching adsorption equilibrium rapidly is crucial to ensure sufficient removal efficiency. While resins generally exhibit high exchange capacities but low exchange rates, fibers provide relatively low adsorption capacities under equivalent volumes but boast high adsorption rates. Chelating fibers show exceptional promise as a material for brine secondary refining in the chlor-alkali industry, especially considering that the concentration of ions such as Ca^{2+} , Mg^{2+} , and Sr^{2+} in incoming water is in the parts-per-million range. This necessitates a relatively low adsorption capacity while emphasizing removal efficiency.

Our laboratory has a strong focus on research related to ion-exchange fibers and chelating fibers. In our previous work, we successfully developed high-amino-containing and high-performance amino fibers [41,42]. Notably, we also prepared a high-amino-containing phosphoric acid fiber based on these amino fibers, demonstrating exceptional capabilities for removing Ca^{2+} and Mg^{2+} ions [43]. Despite these promising results, we observed that the adsorption selectivity of this fiber for Sr^{2+} was not satisfactory during practical applications. Therefore, our current objective is to overcome this limitation by developing an enhanced amino carboxylic acid fiber with improved adsorption performance and verify its adsorption efficiency for the target ions, namely Ca^{2+} , Mg^{2+} , and Sr^{2+} .

2. Experiments

2.1. Materials and methods

The laboratory-made amino fiber polyacrylonitrile–polyethyleneimine (PAN-PEI), as well as NaHCO_3 , Na_2CO_3 , HCl, NaOH, and chloroacetic acid, were used as received in this study. Additionally, sodium bicarbonate (AR), sodium carbonate (AR), hydrochloric acid (AR), and sodium hydroxide (AR) were procured from Tianjin Ou Boke Chemical Reagent Products Sales Co., Ltd., Tianjin, China. Furthermore, chloroacetic acid (AR) was purchased from Shanghai Macklin Biochemical Co., Ltd., Shanghai, China.

2.2. Synthetic route and reaction mechanism

2.2.1. Synthetic route

The amino fiber PAN-PEI, prepared following the method described in the literature [41,42], was employed as the substrate for the amino-carboxylation reaction to produce the amino-carboxyl fiber. The reaction principle underlying the transformation from PAN-PEI to the amino-carboxyl fiber PAN-C-Na is shown in Fig. 1.

2.3. Preparation of amino acid–carboxylic acid fibers

The PAN-C-Na fibers were prepared: 40 g of PAN-PEI fibers were accurately weighed and placed in a 20 L round-bottom flask. Subsequently, 69.4 g of pure chloroacetic acid was dissolved in a 10% NaHCO_3 solution (1 L) to release CO_2 , followed by the addition of 200 mL of 20% Na_2CO_3 solution to the mixture. The resulting solution was carefully poured into the flask, and 9 L of deionized water was added. The reaction was conducted under boiling conditions for 5.5 h, followed by the cessation of heating. After natural cooling, the fibers were removed from the flask and washed three times with distilled water. Subsequently, the fibers were soaked in 1 mol/L HCl for cleaning and then washed with deionized water. The fibers were further immersed in approximately 4 L of 0.5% NaOH solution, washed again with deionized water, and then dried through centrifugation. This process resulted in the formation of chelating fibers of iminodiacetic-acid-type amino acid–carboxylic acid sodium (PAN-C-Na).

2.4. Characterization

2.4.1. Elemental analysis (EA)

CHNSO analysis was performed using the vario EL cube method on a Elementar elemental analyzer (Germany). The presence of Na was measured using the Agilent ICPOES 730 (United States) instrument combined with an American inductively coupled plasma (ICP) atomic emission spectrometer.

2.4.2. Fourier-transform infrared spectroscopy

Fourier-transform infrared spectroscopy analysis was conducted on PAN-PEI, PAN-PEI-Na, PAN-C, and PAN-C-Na. Each sample was ground with KBr at a weight ratio of 1:100, pressed into tablets, and then subjected to Fourier-transform infrared spectroscopy (Spectrum Two, Manufactured by Perkin Elmer, USA) in the range of 4,000–500 cm^{-1} .

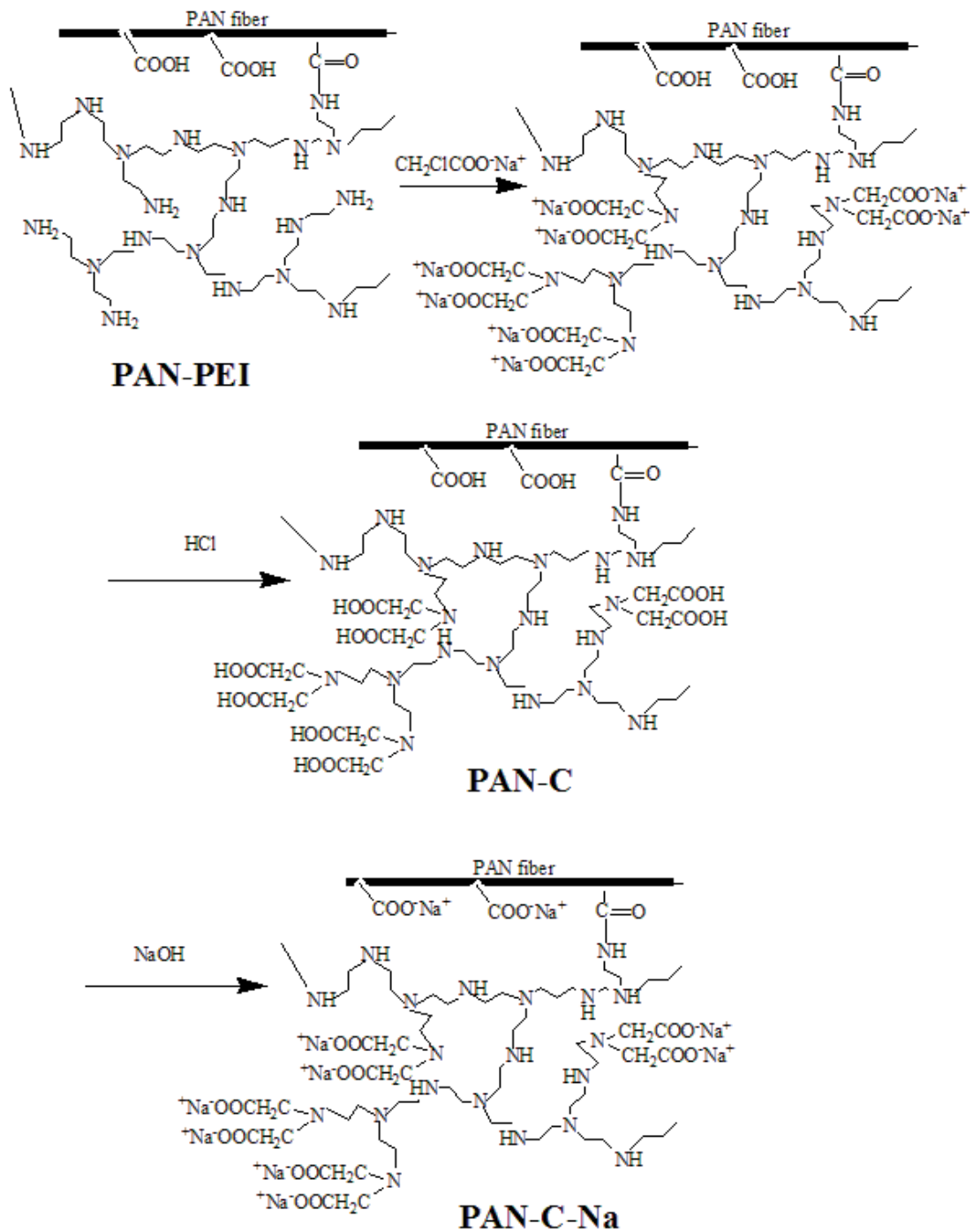


Fig. 1. Schematic diagram of the reaction's pathway from PAN-PEI to PAN-C-Na.

2.4.3. Scanning electron microscopy and energy-dispersive X-ray spectroscopy

Scanning electron microscopy (SEM) and energy-dispersive X-ray spectroscopy analyses were performed on the fibers using a Hitachi SU8010 cold field emission SEM (Japan) with a Sedona SD Detector (Model: SDD3030-300C+) (Sedona Technologies, U.S.-Based Company). Prior to surface morphology analysis, the fibers were mounted on a conductive adhesive and gold sputtered. For cross-sectional morphology

scanning, fiber samples were embedded in hot-melt adhesive, cut into slices with a blade, and then carefully separated and cut into 1-mm-thick sections. These sections were subsequently attached to conductive adhesive and gold sputtered.

2.4.4. Thermal analysis

A thermogravimetric analysis of PAN-PEI and PAN-C-Na was conducted using an STA 449 F5/F3 Jupiter (Netzsch, Germany). These measurements were performed

at a constant heating rate of 10°C/min in a temperature range of 30°C–600°C under a nitrogen flow of 50 mL/min.

2.5. Fiber adsorption testing of Ca^{2+} , Mg^{2+} , and Sr^{2+}

Solutions containing the desired concentrations of Ca^{2+} or Mg^{2+} were prepared by directly dissolving calcium chloride (CaCl_2) or magnesium chloride hexahydrate ($\text{MgCl}_2 \cdot 6\text{H}_2\text{O}$) in deionized water. Adsorption rate experiments were conducted by suspending 0.75 g of PAN-C-Na in 250 mL solutions containing Ca^{2+} or Mg^{2+} at room temperature under continuous stirring. Isothermal adsorption experiments were performed by suspending 0.30 g of PAN-C-Na in 100 mL solutions containing Ca^{2+} or Mg^{2+} at room temperature under continuous stirring. Competitive adsorption experiments for $\text{Ca}^{2+}/\text{Mg}^{2+}/\text{Sr}^{2+}$ were conducted by suspending 0.30 g of PAN-C-Na or PAN-PNa in 100 mL solutions containing Ca^{2+} , Mg^{2+} , and Sr^{2+} at room temperature under continuous stirring. The concentration of metal ions in the water phase was measured using an inductively coupled plasma atomic emission spectrometer (ICAP 7000 Series, Thermo Fisher Scientific, American Company). The adsorption amount of metal ions was calculated using Eq. (1):

$$Q = (C_0 - C_e) \times V \times \frac{1}{mM}$$

where Q is the chelation adsorption capacity (mmol/g), C_0 is the concentration of $\text{Ca}^{2+}/\text{Mg}^{2+}$ before adsorption (mg/L), C_e is the concentration of $\text{Ca}^{2+}/\text{Mg}^{2+}$ after adsorption (mg/L), V is the solution volume (L), M is the molar mass of Ca/Mg (g/mol), and m is the fiber mass (g).

3. Results and discussion

3.1. Elemental analysis results

The elemental composition distribution for two fiber types, PAN-PEI-Na (sodium-type precursor of PAN-PEI) and PAN-C-Na, before and after carboxylation, is presented

in Table 1. Notably, a substantial increase in the proportion of oxygen (O) was observed, indicating the successful conversion of amines to carboxylic acid.

3.2. Infrared comparative analysis

The infrared spectra in Fig. 2 reveal that both PAN-PEI and PAN-PEI-Na exhibit a broad absorption peak in the 1,120–1,030 cm^{-1} range before the reaction, primarily attributed to stretching vibrations of the C–N bond in tertiary and secondary amines within the fibers. Following the reaction, the secondary amine peak at 1,120–1,110 cm^{-1} diminished substantially, accompanied by the emergence of a sharper peak at 1,071 cm^{-1} . This shift resulted from the substitution of two hydrogens of the primary amine by carboxylic acid, thereby forming OOC-N(R)-COO and new tertiary amines. Simultaneously, a few of the hydrogen atoms of the secondary amine were replaced by carboxyl groups, generating $\text{N(R}_1\text{R}_2)\text{-COO}$ tertiary amines. Consequently, there was a marked increase in tertiary amines and a decrease in secondary amines. The successful formation of amino carboxylic acid groups was confirmed by the infrared analysis.

3.3. SEM results and analysis

Fig. 3 presents the cross-sectional energy-dispersive spectra of the PAN-C-Na fiber before and after Ca^{2+} adsorption. Fig. 3A–C depict the elemental distribution of the fiber before adsorption. Fig. 3A presents a SEM image of the fiber cross-section, Fig. 3B illustrates the Na distribution, and

Table 1
Elemental analyses of PAN-PEI-Na, PAN-C-Na fibers

Sample	C/% (m/m)	H/% (m/m)	N/% (m/m)	O/% (m/m)	Na
PAN-PEI-Na	52.37	7.48	19.58	18.79	1.78
PAN-C-Na	47.33	6.42	13.9	28.45	3.90

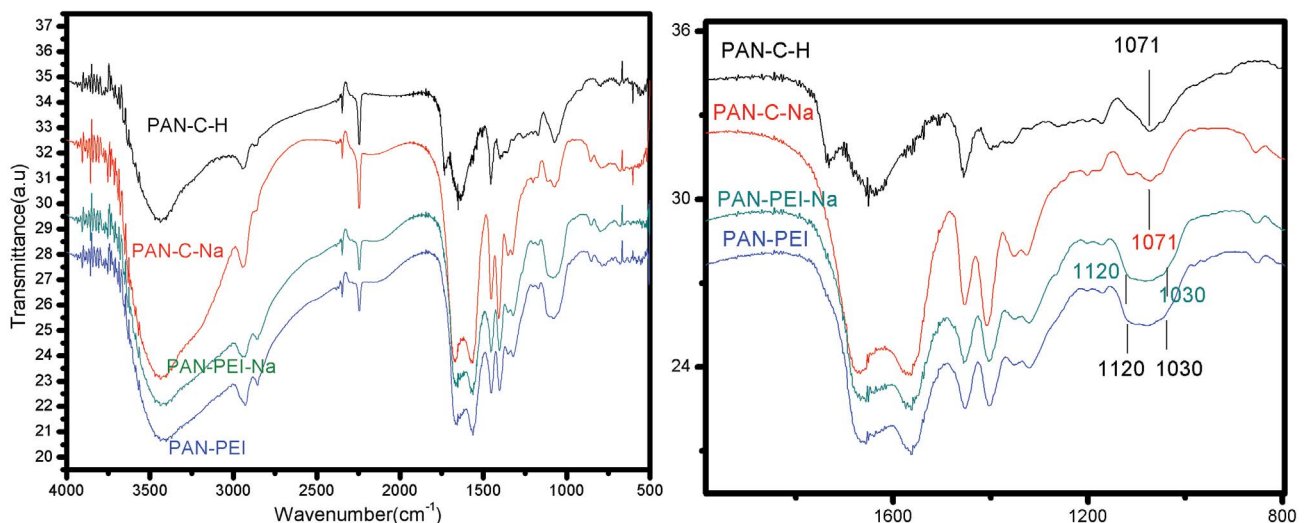


Fig. 2. Infrared spectra of P, PAN-C-H, PAN-C-Na, PAN-PEI-Na, and PAN-PEI.

Fig. 3C depicts the Ca distribution. On comparing Fig. 3B and C, it is evident that before Ca^{2+} adsorption, Na was densely distributed across the fiber cross-section, whereas Ca was sparsely and randomly distributed, resembling noise. Fig. 3D–F display the elemental distribution of the fiber after Ca^{2+} adsorption; specifically, the figures present an SEM image of the fiber cross-section, the Na distribution, and the Ca distribution, respectively. Furthermore, upon comparing Fig. 3E and F, it becomes apparent that after Ca^{2+} adsorption, Na was sparsely distributed in the fiber cross-section, while Ca was more densely distributed, exhibiting a discernible pattern.

Fig. 4 presents the SEM images of the surface and cross-section of the PAN-C-Na fiber. Specifically, Fig. 4A and B depict SEM images of the fiber surface, and Fig. 4C and D present SEM images of the fiber cross-section. Notably, the fiber cross-section exhibits a dumbbell shape, with a width of approximately $10\ \mu\text{m}$ at both ends of the dumbbell and a length of approximately $20\ \mu\text{m}$. Under high magnification, dense grooves are visible on the fiber surface, and the internal porosity can be clearly observed in the cross-section. Additionally, the fiber demonstrates considerable volume expansion when wetted, indicating that upon exposure to the fiber, the solvent infiltrated its internal pores, causing swelling.

3.4. Analysis of thermal analysis results

Fig. 5 displays the differential thermogravimetry curves for PAN-PEI and PAN-C-Na. Notably, PAN-C-Na loses moisture between 30°C – 130°C , and further thermal degradation owing to polymer decomposition was observed over a wide temperature range, from 260°C to 450°C for PAN-C-Na with a peak at 354.4°C and from 300°C to 450°C for PAN-PEI with a peak at 374.3°C . This indicates that both the precursor material and the modified amino-carboxylic acid fibers possess high thermal stability below 260°C .

3.5. Adsorption rate

During the initial stage of adsorption, samples were taken every 30 s, and the results demonstrated that reaction equilibrium was attained within 30 s of the adsorption process (Fig. 6). Furthermore, the adsorption rate was exceptionally high, indicating the suitability of this material for rapid ion adsorption. This favorable kinetic behavior is crucial for efficient deep processing and purification, as it ensures that the performance of the material can be fully harnessed without significant losses due to slow reaction equilibrium.

The high adsorption rate of the chelating fiber is primarily attributed to the concentrated presence of effective functional groups on the fiber surface. Additionally, the hydrophilic swelling property of the modified fiber creates flexible and large pore channels within the swollen fiber, significantly enhancing ion diffusion.

The exchange process of Ca^{2+} and Mg^{2+} ions with sodium and amino phosphate ions on the fiber proceeded through five stages. First, the ion exchange process was initiated through a membrane diffusion process, in which the ions passed through a stationary liquid film surrounding the fibers before reaching the solid surface. Second, the Ca^{2+} and Mg^{2+} ions migrated from the surface of the fiber into the interior, reaching the exchange position. This is referred to as the intra-diffusion process. Third, the Ca^{2+} and Mg^{2+} ions underwent a chemical exchange with sodium ions. Fourth, the sodium ions moved from the inner region of the fiber to the surface. Finally, the sodium ions diffused through the liquid membrane from the fiber surface and into the external solution. While Steps 1 and 5 in the ion adsorption process were controlled by membrane diffusion, Steps 2 and 4 entailed inner pore diffusion. As Step 3 proceeded rapidly, the entire process was primarily controlled either by inner pore diffusion or membrane diffusion. Notably, owing to the flexible and highly connected diffusion channels of the chelating fiber, inner pore diffusion was substantially enhanced.

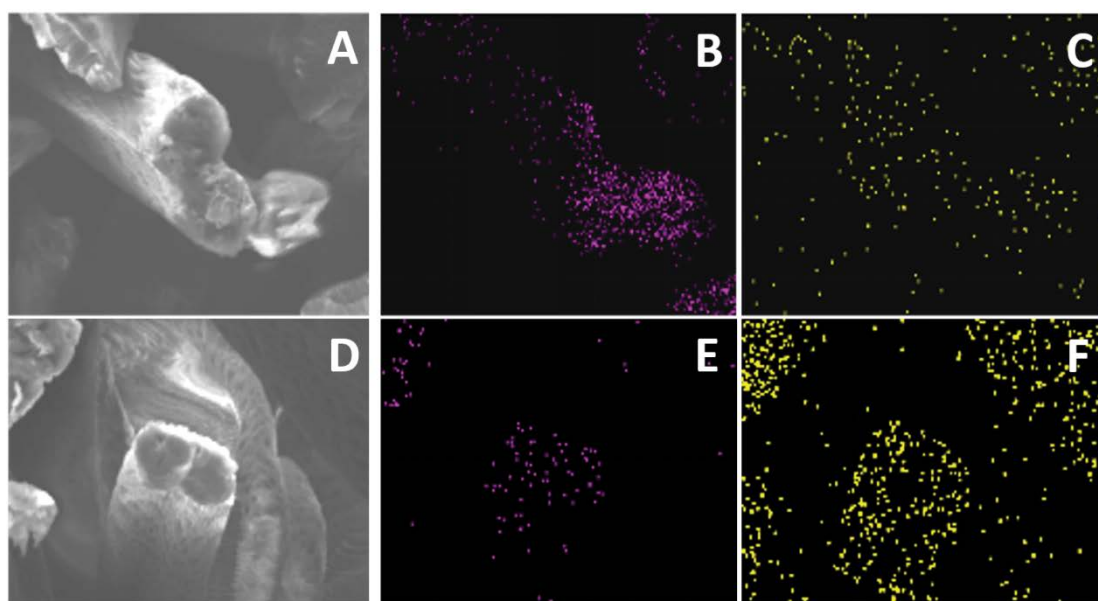


Fig. 3. Cross-sectional energy-dispersive X-ray spectroscopy of PAN-C-Na before and after adsorption for Ca^{2+} .

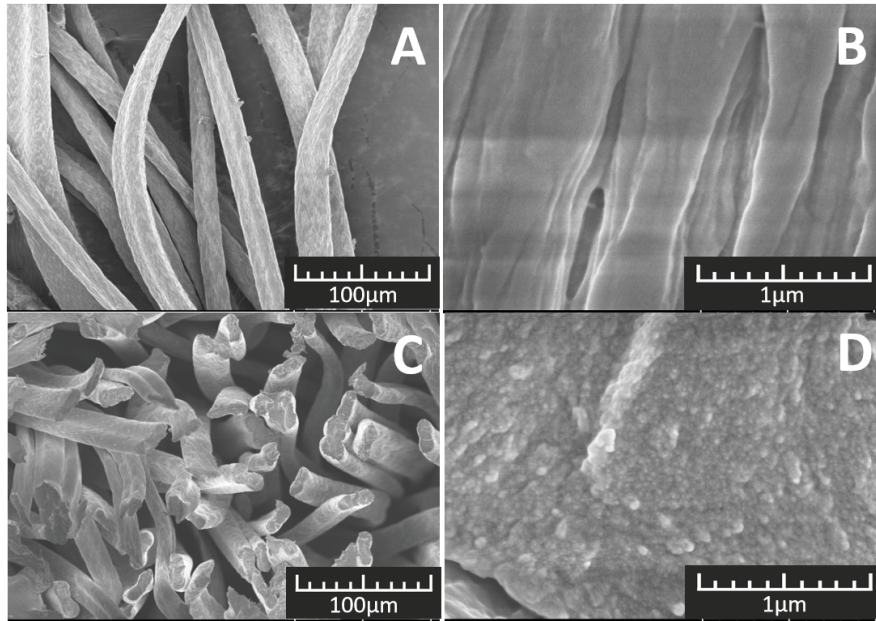


Figure 4. Surface and cross-sectional SEM of PAN-C-Na

Fig. 4. Surface and cross-sectional scanning electron microscopy of PAN-C-Na.

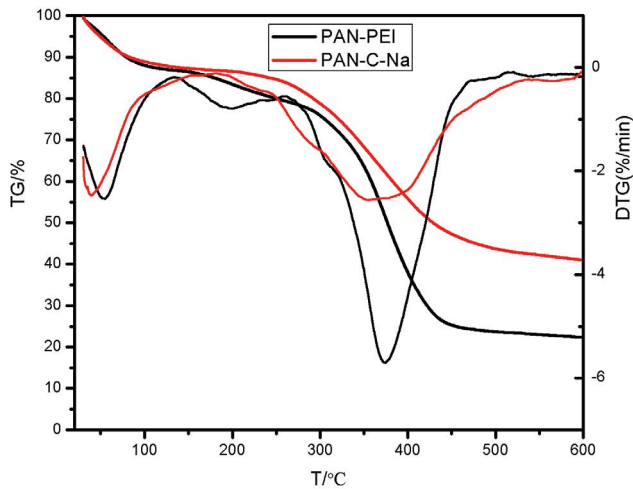


Fig. 5. Differential thermogravimetry curves for PAN-PEI and PAN-C-Na.

Furthermore, the internal swelling generated numerous microfibrils that formed a secondary structure, and the rough fiber surface reduced the diffusion film thickness, thereby promoting the membrane diffusion rate [43]. Thus, because of its small diameter and the presence of microfibrils that reduce resistance to membrane diffusion, the chelating fiber exhibited excellent ion-adsorption performance.

3.6. Adsorption capacity

The $\text{Ca}^{2+}/\text{Mg}^{2+}$ adsorption capacity of PAN-C-Na at various equilibrium concentrations is shown in Table 2. For Ca^{2+} , the observed saturation adsorption capacity was approximately 0.80 mmol/g. Notably, when the equilibrium

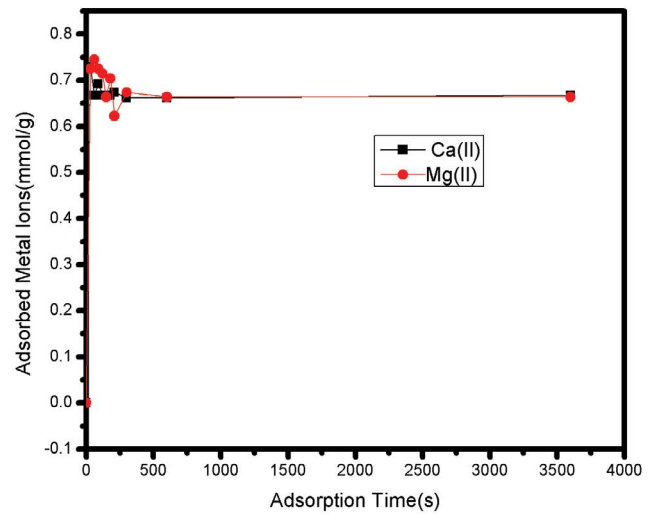


Fig. 6. Adsorption rates of metal ions by PAN-C-Na. Adsorption conditions: initial concentration of metal ions 400 mg/L; pH: 5.5; temperature: 25°C.

concentration was below 0.02 mg/L, the adsorption capacity remained relatively high, reaching at least 0.40 mmol/g. Thus, even at ultralow ion concentrations, PAN-C-Na maintained a high adsorption capacity. Similarly, for Mg^{2+} , the measured saturation adsorption capacity was approximately 0.70 mmol/g. Even for equilibrium concentrations below 0.02 mg/L, an adsorption capacity of at least 0.36 mmol/g was maintained, demonstrating a consistently high adsorption capacity.

The adsorption of calcium and magnesium ions on the amino carboxylic acid fibers is governed by chelation,

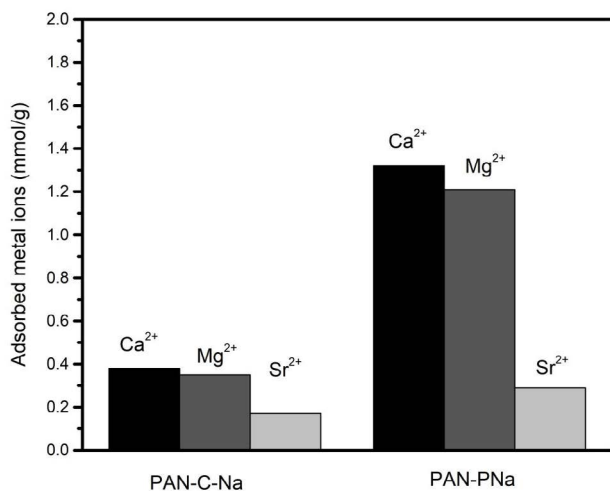


Fig. 7. Comparison of metal ion adsorption capacities on PAN-C-Na. pH: 5.5; initial concentrations of metal ions: 400 mg/L; temperature: 25°C.

wherein the adsorption is directly proportional to the number of active sites available on the fiber. Consequently, the equilibrium adsorption is akin to monolayer adsorption, and the process aligns with Langmuir adsorption [42]. The high chelation constant leads to a large Langmuir adsorption constant, enabling the system to approach saturation even at low concentrations and maintain robust adsorption even at ultralow concentrations.

3.7. Selective adsorption of Ca²⁺, Mg²⁺, and Sr²⁺

As depicted in Fig. 7, when exposed to a mixed solution with an initial concentration of 400 mg/L, the adsorption capacities of PAN-C-Na for Ca, Mg, and Si were found to be 0.38, 0.35, and 0.17, respectively. On the other hand, the adsorption capacities of PAN-PNa for Ca, Mg, and Si were higher, measuring 1.32, 1.21, and 0.29, respectively. The adsorption ratios were found to be 1:0.92:0.44 for PAN-C-Na, compared to 1:0.92:0.22 for PAN-PNa. In the context of the chlor-alkali industry, calcium-magnesium solutions typically contain a certain amount of Sr²⁺, necessitating thorough purification. Notably, PAN-C-Na demonstrates twice the selectivity for Sr²⁺ adsorption compared to the Sr²⁺ selectivity of PAN-PNa. As a result, PAN-C-Na proves to be more effective in adsorbing residual Sr²⁺ ions in practical applications. To achieve optimal results, this material can either be utilized independently or in conjunction with amino-phosphonic acid fibers.

4. Conclusion

Through the application of amine carboxylation to lab-synthesized PAN-PEI fibers, we successfully developed amine carboxyl fibers with uniform functional groups. These fibers exhibit exceptional performance by achieving equilibrium adsorption for Ca²⁺ and Mg²⁺ ions within a remarkable 30 s timeframe, maintaining high adsorption capacities even at ultralow concentrations below 0.02 mg/L. Additionally,

the fibers demonstrate a significant advancement in Sr²⁺ adsorption selectivity compared to amino-phosphonic acid fibers, making them an ideal material for deep purification in the chlor-alkali industry. This industry demands materials with high adsorption capacities, ultrafast adsorption rates for Ca²⁺ and Mg²⁺, and the selective removal of residual Sr²⁺. Future research should focus on increasing the functional group density to further enhance adsorption capacity and optimize the performance of this promising material in real-world applications.

References

- [1] J. Wan, G. Zhu, G. Li, Y. He, Study on the technic of Kai Film Brine Refined, *J. Salt Chem. Ind.*, 4 (2006) 1–3&9.
- [2] Z. Ong, Y. Zhang, R. Cai, L. Wang, Q. Zhang, X. Huang, Study on Ca²⁺, Mg²⁺ removal from salt type brine by NaOH and Na₂CO₃ for saltwater production by nanofiltration, *J. Salt Chem. Ind.*, 4 (2013) 17–19.
- [3] H. Zhao, Operation essentials for calcium/magnesium ion adsorption by chelating resin, *Guangzhou Chem. Ind.*, 13 (2011) 24–26.
- [4] M.F.C. Arias, L.V. i Bru, D.P. Rico, P.V. Galvañ, Comparison of ion exchange resins used in reduction of boron in desalinated water for human consumption, *Desalination*, 278 (2011) 244–249.
- [5] M. Arias-Paic, K.M. Cawley, S. Byg, F.L. Rosario-Ortiz, Enhanced DOC removal using anion and cation ion exchange resins, *Water Res.*, 88 (2016) 981–989.
- [6] R.E. Barker, K. Nuttall, G.J. Millar, Softening of coal seam gas associated water with aluminium exchanged resins, *J. Water Process Eng.*, 21 (2018) 27–43.
- [7] M.A.N. Camacho, A.I.G. López, A. Martínez-Ferez, J.M. Ochando-Pulido, Two-phase olive-oil washing wastewater treatment plus phenolic fraction recovery by novel ion exchange resins process modelling and optimization, *Sep. Purif. Technol.*, 269 (2021) 118755, doi: 10.1016/j.seppur.2021.118755.
- [8] M. Coca, S. Mato, G. González-Benito, M. Ángel Uruñea, M.T. García-Cubero, Use of weak cation exchange resin Lewatit S 8528 as alternative to strong ion exchange resins for calcium salt removal, *J. Food Eng.*, 97 (2010) 569–573.
- [9] Y. Fang, S. Zuo, X. Liang, Y. Cao, X. Gao, Z. Zhang, Preparation and performance of desiccant coating with modified ion exchange resin on finned tube heat exchanger, *Appl. Therm. Eng.*, 93 (2016) 36–42.
- [10] M. Figueira, M. Reig, M. Fernández de Labastida, J.L. Cortina, C. Valderrama, Boron recovery from desalination seawater brines by selective ion exchange resin, *J. Environ. Manage.*, 314 (2022) 114984, doi: 10.1016/j.jenvman.2022.114984.
- [11] J.A. Korak, A.L. Mungan, L.T. Watts, Critical review of waste brine management strategies for drinking water treatment using strong base ion exchange, *J. Hazard. Mater.*, 441 (2023) 129473, doi: 10.1016/j.jhazmat.2022.129473.
- [12] M. Laikhtman, J. Riviello, J.S. Rohrer, Determination of magnesium and calcium in 30% sodium chloride by ion chromatography with on-line matrix elimination, *J. Chromatogr.*, 816 (1998) 282–285.
- [13] Z.Y. Leong, J. Zhang, S. Vafakhah, M. Ding, L. Guo, H.Y. Yang, Electrochemically activated layered manganese oxide for selective removal of calcium and magnesium ions in hybrid capacitive deionization, *Desalination*, 520 (2021) 115374, doi: 10.1016/j.desal.2021.115374.
- [14] C. Boonpanaid, K. Piyamongkala, Using commercial resin for ion exchange to remove hardness from domestic water supply, *Mater. Today: Proc.*, (2023), doi: 10.1016/j.matpr.2023.04.117 (in Press).
- [15] J. Liu, X. Qin, X. Feng, F. Li, J. Liang, D. Hu, Additive-optimized micro-structure in cellulose acetate butyrate-based reverse osmosis membrane for desalination, *Chemosphere*, 327 (2023) 138512, doi: 10.1016/j.chemosphere.2023.138512.

- [16] Z. Mo, D. Li, Q. She, Semi-closed reverse osmosis (SCRO): a concise, flexible, and energy-efficient desalination process, *Desalination*, 544 (2022) 116147, doi: 10.1016/j.desal.2022.116147.
- [17] R. Saeed, A.H. Konsowa, M.S. Shalaby, M.S. Mansour, M.G. Eloffy, Optimization of integrated forward-reverse osmosis desalination processes for brackish water, *Alexandria Eng. J.*, 63 (2023) 89–102.
- [18] N.T. Thu, S. Patra, A. Pranudta, T.T. Nguyen, M.M. El-Moselhy, S. Padungthon, Desalination of brackish groundwater using self-regeneration hybrid ion exchange and reverse osmosis system (HSIX-RO), *Desalination*, 550 (2023) 116378, doi: 10.1016/j.desal.2023.116378.
- [19] X. Zhang, J. Jiang, F. Yuan, W. Song, J. Li, D. Xing, L. Zhao, W. Dong, X. Pan, X. Gao, Estimation of water footprint in seawater desalination with reverse osmosis process, *Environ. Res.*, 204 (2022) 112374, doi: 10.1016/j.envres.2021.112374.
- [20] S.K.A. Al-Amshawee, M.Y.B.M. Yunus, Electrodialysis desalination: the impact of solution flowrate (or Reynolds number) on fluid dynamics throughout membrane spacers, *Environ. Res.*, 219 (2023) 115115, doi: 10.1016/j.envres.2022.115115.
- [21] F. Giacalone, P. Catrini, L. Gurreri, A. Tamburini, A. Cipollina, G. Micale, A. Piacentino, Exergy analysis of electrodialysis for water desalination: influence of irreversibility sources, *Energy Convers. Manage.*, 258 (2022) 115314, doi: 10.1016/j.enconman.2022.115314.
- [22] S. Honarparvar, R. Al-Rashed, A.G. Winter V, A comprehensive investigation of performance of pulsed electrodialysis for desalination of brackish water, *Desalination*, 547 (2023) 116240, doi: 10.1016/j.desal.2022.116240.
- [23] A. Rajput, P.P. Sharma, S.K. Raj, J. Kumari, M.S. Rathore, V. Kulshrestha, Effect of environmental temperature and applied potential on water desalination performance using electrodialysis, *Mater. Today Chem.*, 20 (2021) 100484, doi: 10.1016/j.mtchem.2021.100484.
- [24] M. Sedighi, M.M. Behvand Usefi, A.F. Ismail, M. Ghasemi, Environmental sustainability and ions removal through electrodialysis desalination: operating conditions and process parameters, *Desalination*, 549 (2023) 116319, doi: 10.1016/j.desal.2022.116319.
- [25] D. Ergenç, J. Feijoo, R. Fort, M. Alvarez de Buergo, Effects of potassium ferrocyanide used for desalination on lime composite performances in different curing regimes, *Constr. Build. Mater.*, 259 (2020) 120409, doi: 10.1016/j.conbuildmat.2020.120409.
- [26] A. Masarwa, D. Meyerstein, N. Daltrophe, O. Kedem, Compact accelerated precipitation softening (CAPS) as pretreatment for membrane desalination II. Lime softening with concomitant removal of silica and heavy metals, *Desalination*, 113 (1997) 73–84.
- [27] W. Cai, M. Wang, G.Q. Yang, J. Li, High-performance nanofiltration membranes with a polyamide-polyester composite layer and a polydopamine surface layer for desalination and dye pollutant removal, *Polymer*, 268 (2023) 125720, doi: 10.1016/j.polymer.2023.125720.
- [28] J. Liu, A.A. Abdirahman, X. Wang, Y. Su, Assembly of polyamide nanofilms for nanofiltration membranes with ultra-high desalination performance, *J. Membr. Sci.*, 671 (2023) 121399, doi: 10.1016/j.memsci.2023.121399.
- [29] W. Song, N. Li, S. Ding, X. Wang, H. Li, Y. Zhang, X. Feng, J. Lu, J. Ding, Nanofiltration desalination of reverse osmosis concentrate pretreated by advanced oxidation with ultrafiltration: response surface optimization and exploration of membrane fouling, *J. Environ. Chem. Eng.*, 9 (2021) 106340, doi: 10.1016/j.jece.2021.106340.
- [30] F. Yao, W. Zhang, D. Hu, S. Li, X. Kong, S. Uemura, T. Kusunose, Q. Feng, Ultra-hydrophilic layered titanate nanosheet-based nanofiltration membrane with ultrafast water transport for low energy consumption desalination, *Desalination*, 544 (2022) 116144, doi: 10.1016/j.desal.2022.116144.
- [31] J. Zhu, W. Meng, Q. Xue, K. Zhang, Two-dimensional sulfonated molybdenum disulfide (S-MoS₂) thin-film nanocomposite nanofiltration membrane for selective desalination, *J. Membr. Sci.*, 676 (2023) 121574, doi: 10.1016/j.memsci.2023.121574.
- [32] A.O. AlSuhaimi, S.M. AlRadaddi, A.K. Al-Sheikh Ali, A.M. Shraim, T.S. AlRadaddi, Silica-based chelating resin bearing dual 8-hydroxyquinoline moieties and its applications for solid phase extraction of trace metals from seawater prior to their analysis by ICP-MS, *Arabian J. Chem.*, 12 (2019) 360–369.
- [33] M. Oikawa, H. Takeuchi, D. Chikyu, T. Ohba, Z.-M. Wang, S. Koura, Insight into the role of ionicity in the desalination and separation of a graphene oxide membrane, *Desalination*, 552 (2023) 116433, doi: 10.1016/j.desal.2023.116433.
- [34] X. Qin, X. Qin, X. Xu, J. Zhao, Y. Gui, H. Guo, J. Mao, Y. Wang, Z. Zhang, The membrane-based desalination: focus on MOFs and COFs, *Desalination*, 557 (2023) 116598, doi: 10.1016/j.desal.2023.116598.
- [35] N.A. Shahrin, N.M. Abounahia, A.M.A. El-Sayed, H. Saleem, S.J. Zaidi, An overview on the progress in produced water desalination by membrane-based technology, *J. Water Process Eng.*, 51 (2023) 103479, doi: 10.1016/j.jwpe.2022.103479.
- [36] H. Yuan, J. Liu, X. Zhang, L. Chen, Q. Zhang, L. Ma, Recent advances in membrane-based desalination: focus on desalination and gas separation, *J. Cleaner Prod.*, 387 (2023) 135845, doi: 10.1016/j.jclepro.2023.135845.
- [37] S. Aly, H. Manzoor, S. Simson, A. Abotaleb, J. Lawler, A.N. Mabrouk, Pilot testing of a novel multi effect distillation (MED) technology for seawater desalination, *Desalination*, 519 (2021) 115221, doi: 10.1016/j.desal.2021.115221.
- [38] A. Bamasag, E. Almatrafi, T. Alqahtani, P. Phelan, M. Ullah, M. Mustakeem, M. Obaid, N. Ghaffour, Recent advances and future prospects in direct solar desalination systems using membrane distillation technology, *J. Cleaner Prod.*, 385 (2023) 135737, doi: 10.1016/j.jclepro.2022.135737.
- [39] F. Mahmoudi, H. Siddiqui, M. Pishbin, G. Goodarzi, S. Dehghani, A. Date, A. Akbarzadeh, Sustainable seawater desalination by permeate gap membrane distillation technology, *Energy Procedia*, 110 (2017) 346–351.
- [40] S. Atkinson, Ion exchangers make brine treatment using chlor-alkali electrolysis more efficient, *Membr. Technol.*, 3 (2019) 8, doi: 10.1016/S0958-2118(19)30058-8.
- [41] Y. Bai, Z. Chen, B. Liu, G. Huang, Structural properties characterization and preparation of crosslinking carboxylic fibers based on polyacrylonitrile fibers, *Chin. Syn. Fiber Ind.*, 243 (2019) 41.
- [42] M. Bai, Z. Chen, G. Huang, D. Liu, Preparation of amine chelating fiber and its adsorption properties for Cu²⁺, *Chin. Syn. Fiber Ind.*, 6 (2017) 28.
- [43] D.-X. Liu, G. Xu, Z.-W. Chen, G.-Q. Huang, M.-H. Wu, Outstanding adsorption characteristics of an aminophosphonic acid chelating fiber for calcium and magnesium ions, *Desal. Water Treat.*, 295 (2023) 64–72.